

Voltage to Calcium Transformation Enhances Direction Selectivity in *Drosophila* T4 neurons

Abhishek Mishra^{1,2}, Alexander Borst^{1,2}, Juergen Haag¹

¹Max Planck Institute for Biological Intelligence (in foundation), Martinsried, Germany;

²Graduate School of Systemic Neurosciences, LMU Munich, Martinsried, Germany

Abstract A critical step in neural information processing is the transformation of membrane voltage into calcium signals leading to transmitter release. However, the effect of voltage to calcium transformation on neural responses to different sensory stimuli is not well understood. Here, we use in vivo two-photon imaging of genetically encoded voltage and calcium indicators, Arclight and GCaMP6f respectively, to measure responses in *Drosophila* direction-selective T4 neurons. Comparison between Arclight and GCaMP6f signals revealed calcium signals to have a significantly higher direction selectivity compared to voltage signals. Using these recordings we build a model which transforms T4 voltage responses to calcium responses. The model reproduces experimentally measured calcium responses across different visual stimuli using different temporal filtering steps and a stationary non-linearity. These findings provide a mechanistic underpinning of the voltage-to-calcium transformation and show how this processing step, in addition to synaptic mechanisms on the dendrites of T4 cells, enhances direction selectivity in the output signal of T4 neurons.

Introduction

In order to guide animal behavior, neurons perform a wide range of computations. Neurons encode information via graded changes in membrane potential or action potential frequency. Mostly they communicate via chemical synapses which requires the release of neurotransmitters. When the presynaptic membrane is sufficiently depolarized, voltage-gated calcium channels open and allow Ca^{2+} to enter the cell (Luo 2020). Calcium entry leads to the fusion of synaptic vesicles with the membrane and release of neurotransmitter molecules into the synaptic cleft (Chapman 2002). As neurotransmitters diffuse across the synaptic cleft, they bind to receptors in the postsynaptic membrane, causing postsynaptic neuron to depolarize or hyperpolarize, passing the information from pre to postsynaptic neurons (Di Maio 2008). Voltage to calcium transformation therefore represents one crucial step in neural information processing and neural computation.

A classic example of neural computation is how *Drosophila* neurons compute the direction of visual motion (Borst *et al.* 2020). In *Drosophila*, visual information is processed in parallel ON (contrast increments) and OFF (contrast decrements) pathways (Joesch *et al.* 2010; Eichner *et al.* 2011). Direction selectivity emerges three synapses downstream of photoreceptors, in T4 and T5 for ON and OFF pathways respectively. Four subtypes of T4 and T5 cells exist, each responding selectively to one of the four cardinal directions (Maisak *et al.* 2013). Amazingly, right at the first stage where direction selectivity emerges, T4 and T5 cells exhibit a high degree of direction selectivity, with no responses to null direction stimuli. This statement is, however, based on calcium

recordings. Whole-cell patch clamp recordings show a somewhat different picture: While preferred direction stimuli also lead to large membrane depolarizations, edges or gratings moving along the null directions elicit smaller but significant responses as well (Wienecke *et al.* 2018; Groschner *et al.* 2022). This hints to an additional processing step where voltage signals are transformed into calcium signals that increases direction selectivity of the cells. In order to study this step systematically, we recorded both voltage and calcium signals in response to a large stimulus set that includes gratings and edges moving along various directions at different speeds and contrasts. Using these data, we build a model that captures the transformation from voltage to calcium by a few linear and non-linear processing steps.

Results

We first expressed the genetically encoded calcium indicator GCaMP6f (Chen *et al.* 2013) in T4 cells projecting to layer 3 of the lobula plate. These cells have upward motion as their preferred direction (PD) and downward motion as their null direction (ND). We also expressed the genetically encoded voltage indicator Arclight (Jin *et al.* 2012) using the same driver line. Arclight's fluorescence decreases with membrane depolarization and increases with membrane hyperpolarization. To compare the voltage and calcium signals, we recorded the neural activity in T4c cells dendrites in medulla layer 10 in response to the same set of stimuli using 2-photon microscopy (Denk *et al.* 1990). The complete stimuli set included square-wave gratings of 30° spatial wavelength moving in 12 different directions, and ON edges moving in PD and ND, at four different speeds ($15^\circ s^{-1}$, $30^\circ s^{-1}$, $60^\circ s^{-1}$, $120^\circ s^{-1}$) and four different contrasts (10%, 20%, 50%, 100%).

In a first set of experiments, we measured the voltage and calcium signals in response to gratings moving in PD and ND at four different speeds (figure 1A). As the grating stimuli consists of alternate bright and dark bars moving in a certain direction, there was a modulation in the Arclight (black traces) and GCaMP6f (red traces) responses to it. The GCaMP6f responses showed modulations only for slower speeds, while Arclight responses revealed modulations also for faster speeds. The response amplitudes were much higher for GCaMP6f ($\approx 2.0\Delta F/F$) compared to Arclight ($\approx -0.06\Delta F/F$). The peak responses (maximum $\Delta F/F$) decreased with increasing stimulus speed both for GCaMP6f and Arclight (figure 1B). To understand if voltage to calcium transformation affects direction selectivity in T4 cells, we compared the responses to gratings moving in PD and ND. GCaMP6f responses in ND were negligible compared to its responses in PD, while for Arclight responses in ND were quite visible. We quantified the direction selectivity using a direction selectivity index (DSI) calculated as the difference of the peak responses to preferred and null direction, divided by the sum of the peak responses (Materials and Methods equation (1)). The results revealed a high degree of direction selectivity of ≈ 0.8 for GCaMP6f at slower velocities, compared to a direction selectivity of ≈ 0.4 for Arclight (figure 1E). For both GCaMP6f and Arclight signals, direction selectivity decreased with increasing velocity.

Next, instead of gratings, we used moving bright edges with all other stimulus parameters remaining the same (figure 1C). As the edge moves upward on the screen, it crosses the receptive field of T4c neurons ($\approx 15^\circ$) only once. Hence, there was only a single peak in the response. The peak response decreased with increasing stimulus speed for GCaMP6f, while the peak response remained almost constant for Arclight throughout all speeds (figure 1D). When comparing edge responses moving along preferred and null directions, GCaMP6f showed negligible responses in null direction while Arclight revealed considerable responses to null direction stimuli. The direction selectivity index was again much higher for GCaMP6f compared to Arclight (figure 1F). Together these results show that GCaMP6f signals have a high level of direction selectivity compared to Arclight signals, both for grating and edge stimuli.

The stimulus strength was further varied by changing the contrast between bright and dark bars for gratings and between moving edge and background for edge stimuli. We measured Arclight and GCaMP6f responses to gratings moving at $30^\circ s^{-1}$ at four different contrasts (figure 2A). Increasing contrast resulted in an increase in response for both Arclight and GCaMP6f. GCaMP6f

91 signals were modulated at the temporal frequency of the grating but showed an additional rise
 92 over time. This slow increase was not observed in Arclight signals. We also measured Arclight and
 93 GCaMP6f responses to ON edges moving at the same speed of $30^\circ s^{-1}$ but having different contrasts
 94 (figure 2C). The peak response (maximum $\Delta F/F$) increased with increasing contrast (figure 2D).
 95 Similar to previous experiments, the direction selectivity index was much higher for GCaMP6f (≈ 0.9)
 96 compared to that for Arclight (≈ 0.4) (figure 2E,F).

97 In the results presented so far we compared responses for two directions only, i.e. along the
 98 preferred (upward) and along the null direction (downward). We next extended the comparison to
 99 motion along 12 directions, from 0° to 360° in steps of 30° . For this comparison, we determined the
 100 normalized peak responses of Arclight and GCaMP6f signals to gratings moving in 12 directions
 101 at 4 different speeds and 4 different contrasts, respectively (figure 3A, B). The directional tuning
 102 was much sharper for GCaMP6f compared to Arclight. To quantify this we calculated the directional
 103 tuning index L_{dir} (Mazurek *et al.* 2014) for each speed and each contrast as the vector sum of the
 104 peak responses divided by the sum of all individual vector magnitudes (Materials and Methods
 105 equation (2)). In general, the directional tuning indices again were much higher for GCaMP6f (≈ 0.6)
 106 compared to that of Arclight (≈ 0.2) (figure 3C, D). Together these results show that GCaMP6f signals
 107 have a higher degree of directional tuning across different speeds and contrasts than Arclight.

108 How does the voltage to calcium transformation lead to calcium signals with significantly higher
 109 directional tuning compared to voltage signals? To address this question, we constructed an
 110 algorithmic model (figure 4) which takes Arclight signals as inputs and outputs GCaMP signal. In
 111 order to find the optimal parameter values, we first defined an error function. For each stimulus
 112 condition, the error was calculated as the sum of the squared difference between the model and
 113 experimental data at each time-point (Materials and Methods equation (3)). There were a total
 114 of 112 stimulus conditions: gratings speed (48), gratings contrast (48), edge speed (8) and edge
 115 contrast (8). The total error amounted to the sum of errors across all stimulus conditions (Materials
 116 and Methods equation (4)). We defined the model error as the total error divided by the power
 117 of the data (Materials and Methods equation (5)). We then found the optimal parameters values
 118 of the model that correspond to the minimum total error using Python SciPy optimize minimize
 119 function (Virtanen *et al.* 2020).

120 We started with a simple model (figure 4A). The model first passes the Arclight signal through
 121 a high-pass filter. The high-pass filter brings the input Arclight signal closer to the actual voltage
 122 signal by removing the slowly fluctuating Arclight indicator dynamics. This is followed by a threshold,
 123 assuming that the voltage changes below a certain threshold does not affect the calcium level in
 124 the cell. Now, few experimental observations which we took into consideration for building up the
 125 model further were as follows : First, the GCaMP6f response to gratings showed modulations only
 126 for slower speeds, whereas Arclight response had modulations even at faster speeds (figure 1A).
 127 This suggests that the GCaMP6f signal is a low-pass filtered version of the Arclight signal. In the
 128 simple model, we used a single low-pass filter followed by a gain and time-shift. Multiplication with
 129 a gain factor was required since GCaMP6f signals have a much higher magnitude compared to
 130 Arclight. Arclight and GCaMP6f responses were recorded from cells in different flies with different
 131 receptive fields, therefore the responses had different phases, and a time-shift was necessary
 132 to align the signals. However, the simple model with single low-pass filter could not reproduce
 133 responses across all stimuli. The model error for the complete dataset fit for the simple model was
 134 around 34%. Specifically, the simple model failed to suppress the ND-responses and to reproduce
 135 the edge responses. The directional tuning index L_{dir} was much smaller for the simple model
 136 compared to the experimental data (figure 5E,F). Second, the GCaMP6f responses in addition to
 137 modulation also had a steady rise over time whereas Arclight signal only had modulations (figure 1A,
 138 2A). For reproducing the edge responses and modulation in grating responses, the model needed
 139 a low-pass filter with a small time constant. However to simulate the steady rise in the grating
 140 signal, a low-pass filter with a large time constant was necessary. Hence, we combined the output
 141 of two low-pass filters. Summing up the low-pass filter outputs did not lead to much improvement.

142 However, combining both outputs from the low-pass filters with a multiplication led to significant
143 decrease in the error. The model error for the multiplicative model (figure 4B) then was only at
144 around 20%.

145 The multiplicative model thus has in total 6 parameters - high-pass filter time constant, threshold,
146 low-pass filter 1 time constant, low-pass filter 2 time constant, gain and shift. The multiplicative
147 model was able to reproduce calcium signals across different visual stimuli (figure 5). It could
148 reproduce both the modulation as well as slow rise in the GCaMP6f signal in response to gratings
149 (figure 5A). The multiplicative model could also reproduce the ON edge speed tuning responses
150 across different speeds (figure 5C,D). The directional tuning index L_{dir} were similar for multiplicative
151 model and experimental data across slower speeds and all contrasts (figure 5E,F).

152 Is the slow rise in GCaMP6f signals over time due to the properties of T4 cells or due to the
153 properties of GCaMP6f? To answer this question we used a faster version of the calcium indicator
154 GCaMP8f (Zhang *et al.* 2020). GCaMP8f was expressed in T4c cells using the same driver line. The
155 experiments were repeated using grating stimuli in 12 directions at 4 speeds and ON edges moving
156 in PD and ND. T4c cells GCaMP8f responses were similar to GCaMP6f responses but faster. As
157 with GCaMP6f, GCaMP8f signals had modulation and slow rise over time. We further compared
158 the model parameters values for GCaMP6f data fit and GCaMP8f data fit (figure 6). The model
159 parameters were similar, but with time constants having smaller values for GCaMP8f as it is a faster
160 indicator. Therefore, the slow rise in the calcium signal is not due to the properties of GCaMP6f
161 indicator.

162 To reproduce the calcium responses for direction-selective T4c cells under all stimuli conditions,
163 a multiplicative model was required. For non-direction-selective cells, what does the voltage to
164 calcium transformation look like, and is the simple model able to replicate the calcium response
165 for these cells? In order to answer this question, we expressed Arclight & GCaMP6f in medulla
166 neurons Mi1 & Tm3 cells, which are both non-direction-selective. Mi1 and Tm3 are pre-synaptic to
167 T4 cells and have ON-center receptive field (Behnia *et al.* 2014; Arenz *et al.* 2017). We measured
168 Mi1, Tm3 Arclight (black) and GCaMP6f (red) responses to gratings moving at 4 different speeds
169 and to gratings moving at 4 different contrasts (figure 7). The gratings were moved in only one
170 direction, since the direction does not affect non-direction-selective cells' responses. Contrary to T4,
171 Mi1 GCaMP6f responses had only modulation without a slow increase over time (figure 7A). Tm3
172 GCaMP responses did not increase over time, and showed only modulation for gratings moving at
173 $15^\circ s^{-1}$. For gratings moving at $30^\circ s^{-1}$ and $60^\circ s^{-1}$, there was an increase in Tm3 GCaMP6f response
174 over time, but the Arclight response also already had a slow increment over time (figure 7A). Similar
175 to T4, the peak response for Mi1 and Tm3 decreased with an increase in speed and increased
176 with an increase in contrast (figure 7B, D). Together, these results show that voltage to calcium
177 transformation causes GCaMP6f response increment over time only for direction-selective T4 cells
178 and not for non-direction-selective Mi1 and Tm3 cells.

179 Next, we used the model described in figure 4 to reproduce Mi1 and Tm3 calcium responses
180 using their Arclight responses. As discussed earlier, the simple model (figure 4A) with single
181 low-pass filter was not able to reproduce T4 calcium responses across all stimuli. However, for
182 Mi1 and Tm3, the simple model with a single low-pass filter was able to reproduce the calcium
183 responses across all stimuli conditions (figure 8). The model also accurately replicated the speed
184 and contrast tuning for Mi1 and Tm3 (figure 8B, D). We further compared the model error for
185 simple and multiplicative model for Mi1, Tm3 and T4c data (figure 9). The model error for Mi1 and
186 Tm3 for simple model was $\approx 6.5\%$ and $\approx 5.9\%$ respectively compared to $\approx 11.9\%$ and $\approx 7\%$ for the
187 multiplicative model. Thus, the simple model already performed well for Mi1 and Tm3 dataset,
188 and changing to multiplicative model did not improve the performance. For the T4c dataset the
189 model error was $\approx 34\%$ and $\approx 21\%$ for the simple and multiplicative model respectively. Hence, the
190 multiplicative model with two low-pass filters performed better for T4c dataset whereas for Mi1 and
191 Tm3 the Simple model with single low-pass filter was sufficient to reproduce the calcium responses.
192 This suggests that voltage-to-calcium transformation is more complex for direction-selective cell T4

193 than for the non-direction-selective cells Mi1 and Tm3.

194 Discussion

195 Neuronal signaling and information processing involves the transformation of membrane voltage
196 into calcium signals, which lead to transmitter release. Computations can occur at different stages in
197 the signaling cascade: 1.) dendritic integration and processing of voltage signals. 2.) transformation
198 from voltage to calcium and 3.) between calcium and neurotransmitter release. In this study, we
199 explored the transformation of voltage to calcium in T4-cells, the first direction-selective neurons in
200 the *Drosophila* ON motion vision pathway.

201 We found that the voltage to calcium transformation in T4c neurons enhances their direction
202 selectivity: calcium signals in T4c cells have a significantly higher direction selectivity and tuning
203 compared to membrane voltage across different stimuli conditions (figure 1-3). The direction
204 selectivity index for calcium signals compared with voltage signals for a few stimuli conditions was
205 previously found to be higher in a study in T5 cells using ASAP2f as an optical voltage indicator
206 (Wienecke *et al.* 2018). As calcium is required for neurotransmitter release, this is expected to
207 increase the direction selectivity of T4/T5 cells' output signals. In the lobula plate, T4/T5 cells
208 provide inputs onto large lobula plate tangential cells that are depolarized during preferred and
209 hyperpolarized during null direction motion (Mauss *et al.* 2014). For example, vertical system
210 (VS) cells with dendrites in layer 4 receive direct excitatory inputs from downward tuned T4d/T5d
211 neurons causing depolarization during motion in the downward preferred direction. These VS cells
212 also receive indirect inhibitory inputs from upward tuned T4c/T5c neurons via glutamatergic LPI3-4
213 neurons projecting from layer 3 to layer 4 causing hyperpolarization in VS cells during motion in the
214 upward null direction. Upon silencing LPI3-4 neurons' synaptic output via tetanus toxin, VS neurons
215 depolarization response in the preferred direction did not change, but the null direction response
216 was absent (Mauss *et al.* 2015). This suggests T4/T5 do not release any transmitter in response
217 to null direction motion, which matches our findings for the calcium responses. Thus, voltage to
218 calcium transformation increases direction selectivity in T4/T5 cells and this enhances direction
219 selectivity in downstream neurons.

220 Electrophysiology has been the most frequently used method to measure the membrane
221 potential changes in neurons. However, due to the small size of neurons in the optic lobe, single-cell
222 electrophysiological recordings of these neurons have been difficult. Genetically encoded voltage
223 indicators (GEVIs) have evolved as powerful tools for recording changes in neuronal membrane
224 potentials (Yang *et al.* 2016). Optical methods of monitoring brain activity are appealing because
225 they allow simultaneous, noninvasive monitoring of activity in many individual neurons. We used
226 a fluorescence protein (FP) voltage sensor called ArcLight (Jin *et al.* 2012). ArcLight is based on the
227 fusion of the voltage-sensing domain of *Ciona intestinalis* voltage-sensitive phosphatase (Murata
228 *et al.* 2005) and the fluorescent protein super ecliptic pHluorin with an A227D mutation. ArcLight
229 has been shown to robustly report both subthreshold events and action potentials in genetically
230 targeted neurons in the intact *Drosophila* brain (Cao *et al.* 2013).

231 We built a model to capture voltage to calcium transformation in T4c, Mi1, and Tm3 cells. A
232 simple model with a single low-pass filter was able to reproduce calcium responses in non-direction-
233 selective Mi1 and Tm3 cells (figure 8), whereas a more complex model combining the output of two
234 low-pass filters via a multiplication was required to reproduce T4c calcium responses (figure 5). The
235 direction selectivity for the simple model signals for T4c was lower compared to the multiplicative
236 model. This suggests that voltage-calcium transformation in Mi1 and Tm3 cells is different from
237 those in T4c cells.

238 The time constants for the two low-pass filters were identical for the multiplicative model for
239 T4c data fit. Thus, these two low-pass filters in the multiplicative model could also be replaced by a
240 single low-pass filter followed by a quadratic non-linearity. An exponent of close to 2 (exact value:
241 2.2) was found in the parameter search for a model with a single low-pass filter followed by an
242 exponential nonlinearity.

Differential expression of voltage-gated calcium channels in these cells could explain the different voltage to calcium transformation. Voltage-gated calcium channels mediate depolarization-induced calcium influx that drives the release of neurotransmitters. The $\alpha 1$ -subunit of the voltage-gated calcium channels forms the ion-conducting pore, which makes it distinct from other calcium channels. Three families of genes encode $\alpha 1$ subunits. *Drosophila* genome has one $\alpha 1$ subunit gene in each family: $\alpha 1D$ (Ca_v1), cac (Ca_v2), and $\alpha 1T$ (Ca_v3) (Littleton & Ganetzky 2000; King 2007). In *Drosophila* antennal lobe projection neurons, cac (Ca_v2) type and $\alpha 1T$ (Ca_v3) type voltage-gated calcium channels are involved in sustained and transient calcium currents, respectively (Gu *et al.* 2009; Iniguez *et al.* 2013). According to a RNA-sequencing study (Davis *et al.* 2020), $\alpha 1T$ (Ca_v3) mRNA have higher expression in Mi1 (2050.16 Transcripts per Million (TPM)) compared to T4 (686.68 TPM) and Tm3 (336.45 TPM). While cac (Ca_v2) mRNA have higher expression in T4 (1298.53 TPM) compared to Mi1 (986.25 TPM) and Tm3 (817.61 TPM). Different expression of voltage-gated calcium channels could cause different voltage to calcium transformations in non-direction selective and direction-selective cells. In addition to dendritic integration of postsynaptic voltages, the specific voltage-to-calcium transformation described in this study provides an important processing step that enhances direction selectivity in the output signal of motion-sensing neurons of the fly.

Materials and Methods

Flies

Flies (*Drosophila melanogaster*) were raised at 25°C and 60% humidity on a 12 hour light/12 hour dark cycle on standard cornmeal agar medium. For calcium imaging experiments, genetically-encoded calcium indicator GCaMP6f (Chen *et al.* 2013) was expressed in T4 neurons with axon terminals predominantly in layer 3 of the lobula plate. Similarly for voltage imaging experiments, genetically-encoded voltage indicator Arclight (Jin *et al.* 2012) was expressed in T4 layer 3 neurons. The flies genotype were as follows :

1. T4c>GCaMP6f : w+ ; VT15785-Gal4AD / UAS-GCaMP6f; VT50384-Gal4DBD / UAS-GCaMP6f
2. T4c>Arclight : w+ ; VT15785-Gal4AD / UAS-Arclight; VT50384-Gal4DBD / +

For Mi1 and Tm3 experiments, the flies genotype were as follows :

1. Mi1>GCaMP6f : w+ ; R19F01-Gal4AD / UAS-GCaMP6f; R71D01-Gal4DBD / UAS-GCaMP6f
2. Mi1>Arclight : w+ ; R19F01-Gal4AD / UAS-Arclight; R71D01-Gal4DBD / +
3. Tm3>GCaMP6f : w+ ; R13E12-Gal4AD / UAS-GCaMP6f; R59C10-Gal4DBD / UAS-GCaMP6f
4. Tm3>Arclight : w+ ; R13E12-Gal4AD / UAS-Arclight; R59C10-Gal4DBD / +

Calcium & voltage imaging

For imaging experiments, fly surgeries were performed as previously described (Maisak *et al.* 2013). Briefly, flies were anaesthetized with CO₂ or on ice, fixed with their backs, legs and wings to a Plexiglas holder with back of the head exposed to a recording chamber filled with fly external solution. The cuticula at the back of the head on one side of the brain was cut away with a fine hypodermic needle and removed together with air sacks covering the underlying optic lobe. The neuronal activity was then measured from the optic lobe with a custom-built 2-photon microscope as previously described (Maisak *et al.* 2013). Images were acquired at 64 x 64 pixels resolution and frame rate 13 Hz with the Scanimage software in Matlab (Pologruto *et al.* 2003).

Visual stimulation

For the study of visual responses of T4c cells, visual stimuli were presented on a custom-built projector-based arena as described in (Arenz *et al.* 2017). In brief : Two micro-projectors (TI DLP Lightcrafter 3000) were used to project stimuli onto the back of an opaque cylindrical screen covering 180° in azimuth and 105° in elevation of the fly's visual field. To increase the refresh rate from 60 Hz to 180 Hz (at 8 bit color depth), projectors were programmed to use only green LED

(OSRAM L CG H9RN) which emits light between 500 nm to 600 nm wavelength. Two long-pass filters (Thorlabs FEL0550 and FGL550) were placed in front of each projector to restrict the stimulus light to wavelengths above 550 nm. This prevents overlap between fluorescence signal and arena light spectra. To allow only fluorescence emission spectrum to be detected, a band-pass filter (Brightline 520/35) was placed in-front of the photomultiplier. Stimuli were rendered using custom written software in Python 2.7.

Stimuli

Stimuli were presented with 3-5 repetitions per experiment in a randomized fashion. To measure the directional and speed tuning, square-wave gratings with a spatial wavelength of 30° spanning the full extent of the stimulus arena were used. The gratings were moved in 12 different directions from $0^\circ - 360^\circ$ at 4 different speeds ($15^\circ s^{-1}$, $30^\circ s^{-1}$, $60^\circ s^{-1}$, $120^\circ s^{-1}$). Similarly, to measure direction and contrast tuning, square-wave gratings with a spatial wavelength of 30° spanning the full extent of the stimulus arena were used. The gratings moved at a speed of $30^\circ s^{-1}$ in 12 different directions at 4 different contrasts (10%, 20%, 50%, 100%). Edge responses were measured using ON edge i.e. bright edge moving on a dark background with full contrast. The ON edge moved in preferred direction (upward) or null direction (downward) at 4 different speeds ($15^\circ s^{-1}$, $30^\circ s^{-1}$, $60^\circ s^{-1}$, $120^\circ s^{-1}$).

Data analysis

Data analysis was performed using custom-written routines in Matlab and Python 2.7, 3.7. Images were automatically registered using horizontal and vertical translations to correct for the movement of brain. Fluorescence changes ($\Delta F/F$) were then calculated using a standard baseline algorithm (Jia *et al.* 2011). Regions of interest (ROIs) were drawn on the average raw image manually by hand in the medulla layer M10 for signals from T4 dendrites. Averaging the fluorescence change over this ROI in space resulted in a ($\Delta F/F$) time course. Voltage imaging with Arclight and calcium imaging with GCaMP6f and GCaMP8f were performed and analysed using same settings.

The direction selectivity was evaluated using a direction selectivity index (DSI) calculated as the difference of the peak responses to preferred and null direction, divided by the sum of the peak responses:

$$DSI = \frac{PD_{peak} - ND_{peak}}{PD_{peak} + ND_{peak}} \quad (1)$$

In the above measurement, only the difference in response between the two opposing directions of motion is quantified. To take into account all 12 directions of motion, we calculated the directional tuning index:

$$L_{dir} = \left| \frac{\sum_{\varphi} \vec{v}(\varphi)}{\sum_{\varphi} |\vec{v}(\varphi)|} \right| \quad (2)$$

where $\vec{v}(\varphi)$ is a vector proportionally scaled with the mean response and points in the direction corresponding to the direction of motion given by the rotation angle φ of the stimulus (Mazurek *et al.* 2014).

Model simulations

Custom-written Python3.7 scripts were used to simulate the models (figure 4). To calculate the optimal parameter values, we first defined an error function. For each stimulus condition (s_i), the error was calculated as:

$$error(s_i) = \sum_{t=0}^{t=N} (model(s_i t) - data(s_i t))^2 \quad (3)$$

The model took as input Arclight data across all 112 different stimuli conditions. Next, we summed the error for all stimuli conditions:

$$total\ error = \sum_{i=1}^{i=112} error(s_i) \quad (4)$$

328 The model parameters were initialized with random values within the defined parameter bounds.
 329 Python SciPy optimize minimize function then used the L-BFGS-B (Limited Broyden Fletcher Goldfarb
 330 Shanno) algorithm to find the parameter values corresponding to the minimum total error. A total
 331 of 300 runs were performed, and the parameter values that corresponded to the run with the
 332 lowest error were used to produce the final output signals. To compare the model performances,
 333 we calculated the model error as:

$$\text{model error [\% of data power]} = \frac{\text{total error}}{\sum_{i=1}^{112} (\text{data}(s_i))^2} * 100 \quad (5)$$

334 References

- 335 1. Denk, W., Strickler, J. H. & Webb, W. W. Two-photon laser scanning fluorescence microscopy.
 336 *Science* **248**, 73–76 (1990). doi: [10.1126/science.2321027](https://doi.org/10.1126/science.2321027)
- 337 2. Littleton, J. T. & Ganetzky, B. Ion channels and synaptic organization: analysis of the *Drosophila*
 338 genome. *Neuron* **26**, 35–43 (2000). doi: [10.1016/s0896-6273\(00\)81135-6](https://doi.org/10.1016/s0896-6273(00)81135-6)
- 339 3. Chapman, E. R. Synaptotagmin: a Ca²⁺ sensor that triggers exocytosis? *Nature Reviews Molecu-*
 340 *lar Cell Biology* **3**, 498–508 (2002). doi: [10.1038/nrm855](https://doi.org/10.1038/nrm855)
- 341 4. Pologruto, T. A., Sabatini, B. L. & Svoboda, K. ScanImage: flexible software for operating laser
 342 scanning microscopes. *Biomedical engineering online* **2**, 1–9 (2003). doi: [10.1186/1475-925X-2-13](https://doi.org/10.1186/1475-925X-2-13)
- 343 5. Murata, Y., Iwasaki, H., Sasaki, M., Inaba, K. & Okamura, Y. Phosphoinositide phosphatase
 344 activity coupled to an intrinsic voltage sensor. *Nature* **435**, 1239–1243 (2005). doi: [10.1038/nature03650](https://doi.org/10.1038/nature03650)
- 345 6. King, G. F. Modulation of insect CaV channels by peptidic spider toxins. *Toxicon* **49**, 513–530
 346 (2007). doi: [10.1016/j.toxicon.2006.11.012](https://doi.org/10.1016/j.toxicon.2006.11.012)
- 347 7. Di Maio, V. Regulation of information passing by synaptic transmission: a short review. *Brain*
 348 *research* **1225**, 26–38 (2008). doi: [10.1016/j.brainres.2008.06.016](https://doi.org/10.1016/j.brainres.2008.06.016)
- 349 8. Gu, H. *et al.* Cav2-type calcium channels encoded by cac regulate AP-independent neurotrans-
 350 mitter release at cholinergic synapses in adult *Drosophila* brain. *Journal of neurophysiology*
 351 **101**, 42–53 (2009). doi: [10.1152/jn.91103.2008](https://doi.org/10.1152/jn.91103.2008)
- 352 9. Joesch, M., Schnell, B., Raghu, S. V., Reiff, D. F. & Borst, A. ON and OFF pathways in *Drosophila*
 353 motion vision. *Nature* **468**, 300–304 (2010). doi: [10.1038/nature09545](https://doi.org/10.1038/nature09545)
- 354 10. Eichner, H., Joesch, M., Schnell, B., Reiff, D. F. & Borst, A. Internal structure of the fly elementary
 355 motion detector. *Neuron* **70**, 1155–1164 (2011). doi: [10.1016/j.neuron.2011.03.028](https://doi.org/10.1016/j.neuron.2011.03.028)
- 356 11. Jia, H., Rochefort, N. L., Chen, X. & Konnerth, A. In vivo two-photon imaging of sensory-
 357 evoked dendritic calcium signals in cortical neurons. *Nature protocols* **6**, 28–35 (2011). doi:
 358 [10.1038/nprot.2010.169](https://doi.org/10.1038/nprot.2010.169)
- 359 12. Jin, L. *et al.* Single action potentials and subthreshold electrical events imaged in neurons with a
 360 fluorescent protein voltage probe. *Neuron* **75**, 779–785 (2012). doi: [10.1016/j.neuron.2012.06.040](https://doi.org/10.1016/j.neuron.2012.06.040)
- 361 13. Cao, G. *et al.* Genetically targeted optical electrophysiology in intact neural circuits. *Cell* **154**,
 362 904–913 (2013). doi: [10.1016/j.cell.2013.07.027](https://doi.org/10.1016/j.cell.2013.07.027)
- 363 14. Chen, T.-W. *et al.* Ultrasensitive fluorescent proteins for imaging neuronal activity. *Nature* **499**,
 364 295–300 (2013). doi: [10.1038/nature12354](https://doi.org/10.1038/nature12354)
- 365 15. Iniguez, J., Schutte, S. S. & O'Dowd, D. K. Cav3-type $\alpha 1T$ calcium channels mediate transient
 366 calcium currents that regulate repetitive firing in *Drosophila* antennal lobe PNs. *Journal of*
 367 *neurophysiology* **110**, 1490–1496 (2013). doi: [10.1152/jn.00368.2013](https://doi.org/10.1152/jn.00368.2013)
- 368 16. Maisak, M. S. *et al.* A directional tuning map of *Drosophila* elementary motion detectors. *Nature*
 369 **500**, 212–216 (2013). doi: [10.1038/nature12320](https://doi.org/10.1038/nature12320)
- 370

- 371 17. Behnia, R., Clark, D. A., Carter, A. G., Clandinin, T. R. & Desplan, C. Processing properties of
372 ON and OFF pathways for *Drosophila* motion detection. *Nature* **512**, 427–430 (2014). doi:
373 [10.1038/nature13427](https://doi.org/10.1038/nature13427)
- 374 18. Mauss, A. S., Meier, M., Serbe, E. & Borst, A. Optogenetic and pharmacologic dissection of
375 feedforward inhibition in *Drosophila* motion vision. *Journal of Neuroscience* **34**, 2254–2263
376 (2014). doi: [10.1523/JNEUROSCI.3938-13.2014](https://doi.org/10.1523/JNEUROSCI.3938-13.2014)
- 377 19. Mazurek, M., Kager, M. & Van Hooser, S. D. Robust quantification of orientation selectivity and
378 direction selectivity. *Frontiers in neural circuits* **8**, 92 (2014). doi: [10.3389/fncir.2014.00092](https://doi.org/10.3389/fncir.2014.00092)
- 379 20. Mauss, A. S. *et al.* Neural circuit to integrate opposing motions in the visual field. *Cell* **162**,
380 351–362 (2015). doi: [10.1016/j.cell.2015.06.035](https://doi.org/10.1016/j.cell.2015.06.035)
- 381 21. Yang, H. H. *et al.* Subcellular imaging of voltage and calcium signals reveals neural processing
382 in vivo. *Cell* **166**, 245–257 (2016). doi: [10.1016/j.cell.2016.05.031](https://doi.org/10.1016/j.cell.2016.05.031)
- 383 22. Arenz, A., Drews, M. S., Richter, F. G., Ammer, G. & Borst, A. The temporal tuning of the
384 *Drosophila* motion detectors is determined by the dynamics of their input elements. *Current*
385 *Biology* **27**, 929–944 (2017). doi: [10.1016/j.cub.2017.01.051](https://doi.org/10.1016/j.cub.2017.01.051)
- 386 23. Wienecke, C. F., Leong, J. C. & Clandinin, T. R. Linear summation underlies direction selectivity
387 in *Drosophila*. *Neuron* **99**, 680–688 (2018). doi: [10.1016/j.neuron.2018.07.005](https://doi.org/10.1016/j.neuron.2018.07.005)
- 388 24. Borst, A., Haag, J. & Mauss, A. S. How fly neurons compute the direction of visual motion.
389 *Journal of Comparative Physiology A* **206**, 109–124 (2020). doi: [10.1007/s00359-019-01375-9](https://doi.org/10.1007/s00359-019-01375-9)
- 390 25. Davis, F. P. *et al.* A genetic, genomic, and computational resource for exploring neural circuit
391 function. *Elife* **9**, e50901 (2020). doi: [10.7554/eLife.50901](https://doi.org/10.7554/eLife.50901)
- 392 26. Luo, L. *Principles of Neurobiology* (Garland Science, 2020). doi: [10.1201/9781003053972](https://doi.org/10.1201/9781003053972)
- 393 27. Virtanen, P. *et al.* SciPy 1.0: fundamental algorithms for scientific computing in Python. *Nature*
394 *methods* **17**, 261–272 (2020). doi: [10.1038/s41592-019-0686-2](https://doi.org/10.1038/s41592-019-0686-2)
- 395 28. Zhang, Y. *et al.* jRCaMP1a Fast genetically encoded calcium indicators. *Online resource* (2020).
396 doi: [10.25378/janelia.13148243.v4](https://doi.org/10.25378/janelia.13148243.v4)
- 397 29. Groschner, L. N., Malis, J. G., Zuidinga, B. & Borst, A. A biophysical account of multiplication by
398 a single neuron. *Nature* **603**, 119–123 (2022). doi: [10.1038/s41586-022-04428-3](https://doi.org/10.1038/s41586-022-04428-3)

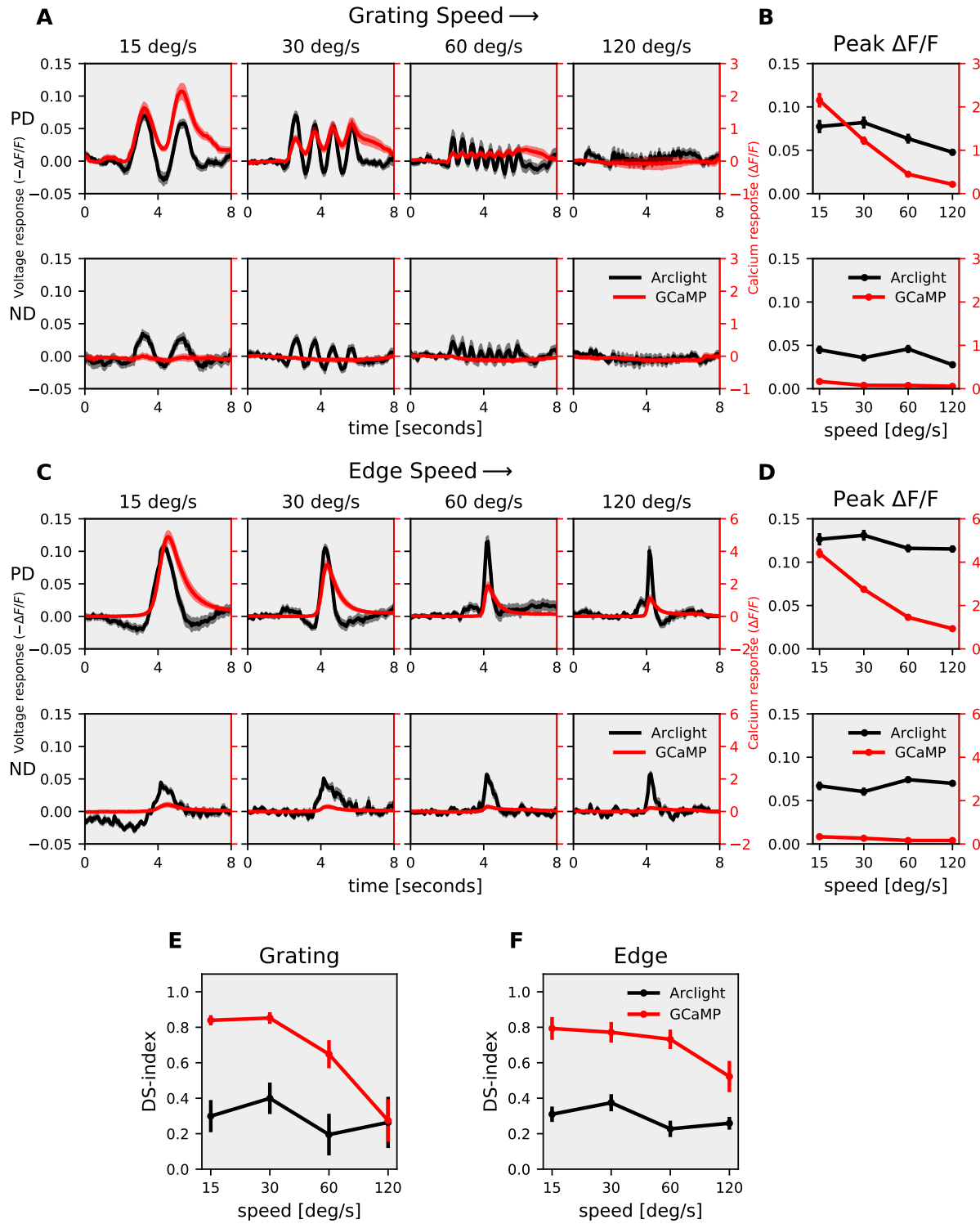


Figure 1. T4c speed dependence : (A) T4c Arclight (black) and GCaMP6f (red) responses to grating moving in PD (top row) and ND (bottom row) at 4 different speeds. The plots have twin y-axis. The left y-axis of the plot represents voltage responses i.e. changes in Arclight fluorescence ($-\Delta F/F$) and the right y-axis of the plot represents calcium responses i.e. changes in GCaMP6f fluorescence ($\Delta F/F$) (B) T4c peak responses to grating moving in PD (top) and ND (bottom) at 4 different speeds. (n = 20 ROIs from N = 10 flies for Arclight, n = 18, N = 9 for GCaMP6f) (C) T4c Arclight (black) and GCaMP6f (red) responses to ON-edge moving in PD (top row) and ND (bottom row) at 4 different speeds. (D) T4c peak responses to ON-edge moving in PD and ND at 4 different speeds. (n = 29, N = 10 for Arclight, n = 17, N = 4 for GCaMP6f) (E) Direction selectivity index (DSI) calculated as difference of peak responses in PD and ND divided by the sum of peak responses for grating. (F) Direction selectivity index (DSI) for ON-edge. All data shows the mean \pm SEM. PD: preferred direction, ND: null direction.

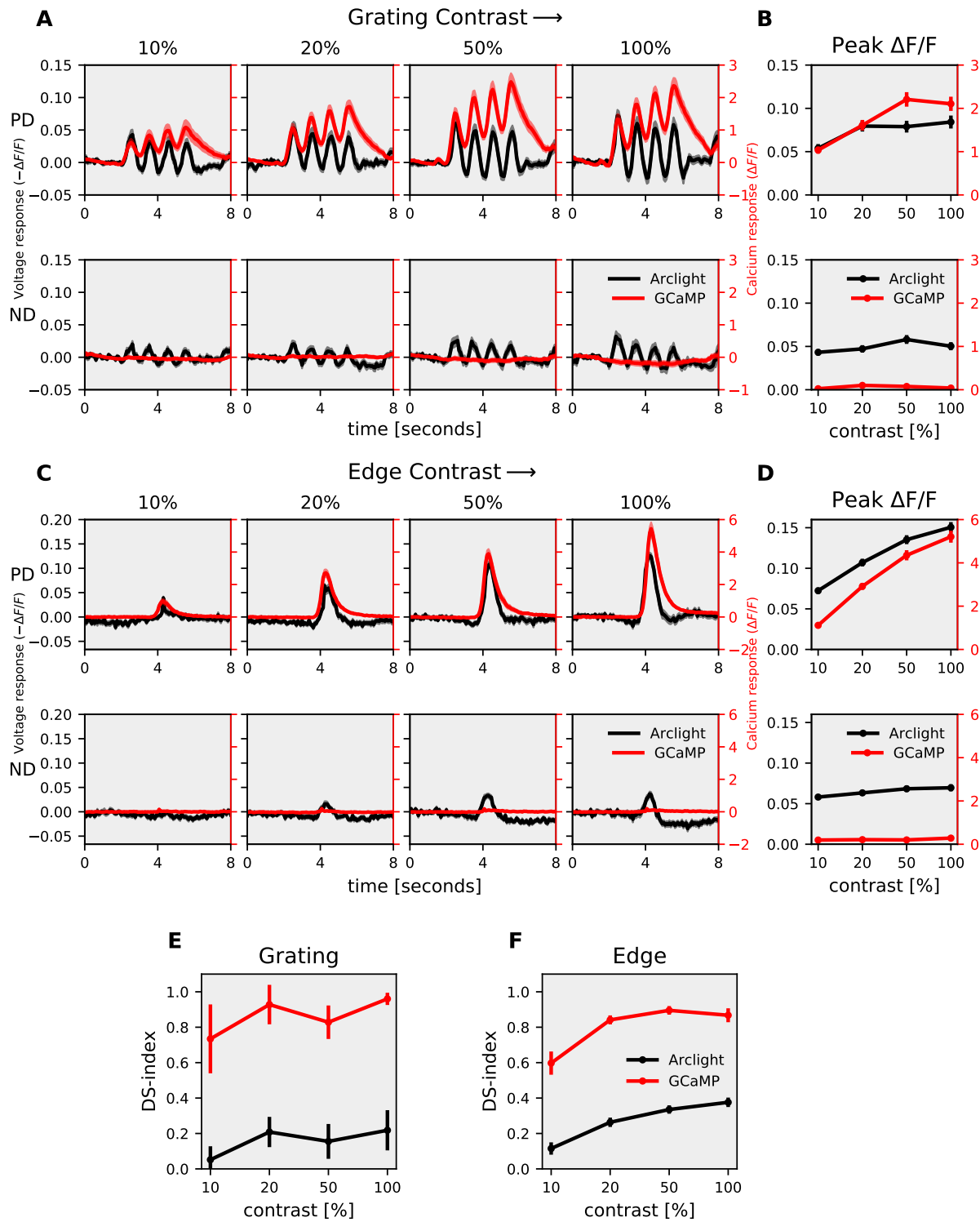


Figure 2. T4c contrast dependence : (A) T4c Arclight (black) and GCaMP6f (red) responses to grating moving in PD (top row) and ND (bottom row) at 4 different contrasts. The left y-axis of the plot represents voltage responses i.e. changes in Arclight fluorescence ($-\Delta F/F$) and the right y-axis of the plot represents calcium responses i.e. changes in GCaMP6f fluorescence ($\Delta F/F$) (B) T4c peak responses to grating moving in PD (top) and ND (bottom) at 4 different contrasts. ($n = 23$ ROIs from $N = 11$ flies for Arclight, $n = 22$, $N = 9$ for GCaMP6f) (C) T4c Arclight (black) and GCaMP6f (red) responses to ON-edge moving in PD (top row) and ND (bottom row) at 4 different contrasts. (D) T4c peak responses to ON-edge moving in PD and ND at 4 different contrasts. ($n = 36$, $N = 5$ for Arclight, $n = 41$, $N = 7$ for GCaMP6f) (E) Direction selectivity index (DSI) calculated as difference of peak responses in PD and ND divided by the sum of peak responses for grating. (F) Direction Selectivity Index (DSI) for ON-edge. All data shows the mean \pm SEM.

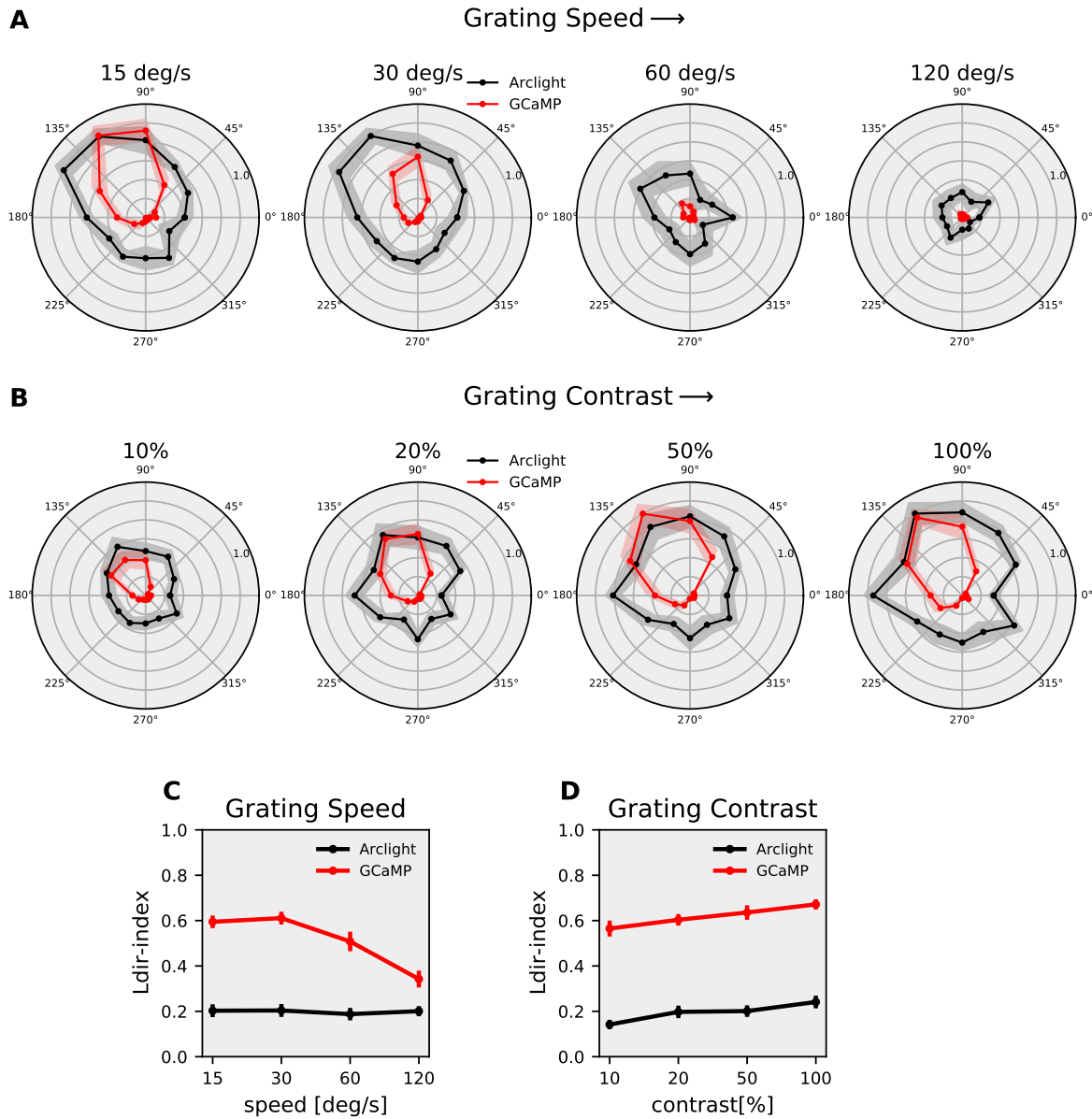


Figure 3. T4c direction tuning : (A) T4c Arclight (black) and GCaMP6f (red) normalized peak responses to grating moving in 12 directions at 4 different speeds. (n = 20 ROIs from N = 10 flies for Arclight, n = 18, N = 9 for GCaMP6f) (B) T4c Arclight (black) and GCaMP6f (red) normalized peak responses to grating moving in 12 directions at 4 different contrasts. (n = 23, N = 11 for Arclight, n = 22, N = 9 for GCaMP6f) (C) The directional tuning index L_{dir} for grating moving at 4 different speeds. The directional tuning index is calculated as the vector sum of the peak responses divided by the sum of all individual vector magnitudes. (D) The directional tuning index for grating at 4 different contrasts. All data shows the mean \pm SEM measured in 5 different flies.

A Simple Model



B Multiplicative Model

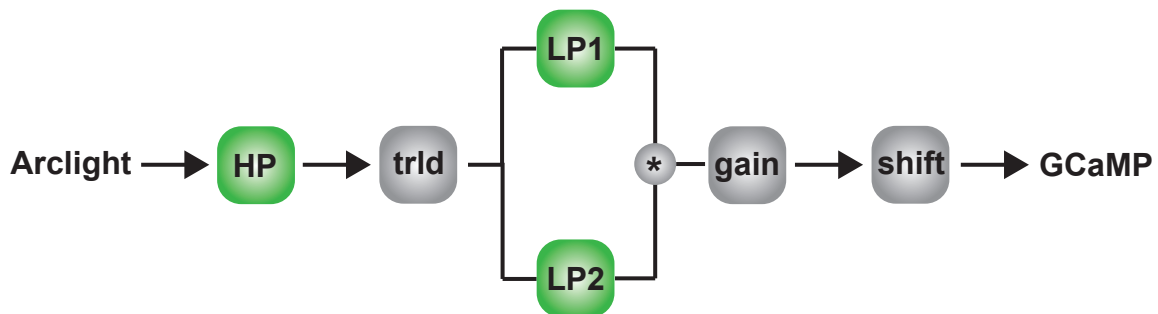


Figure 4. Models for voltage to calcium transformation : (A) Simple model consisting of High-Pass filter (HP), threshold (trld), Low-Pass filter (LP), gain and shift. (B) Multiplicative model combining output of two low-pass filters via multiplication.

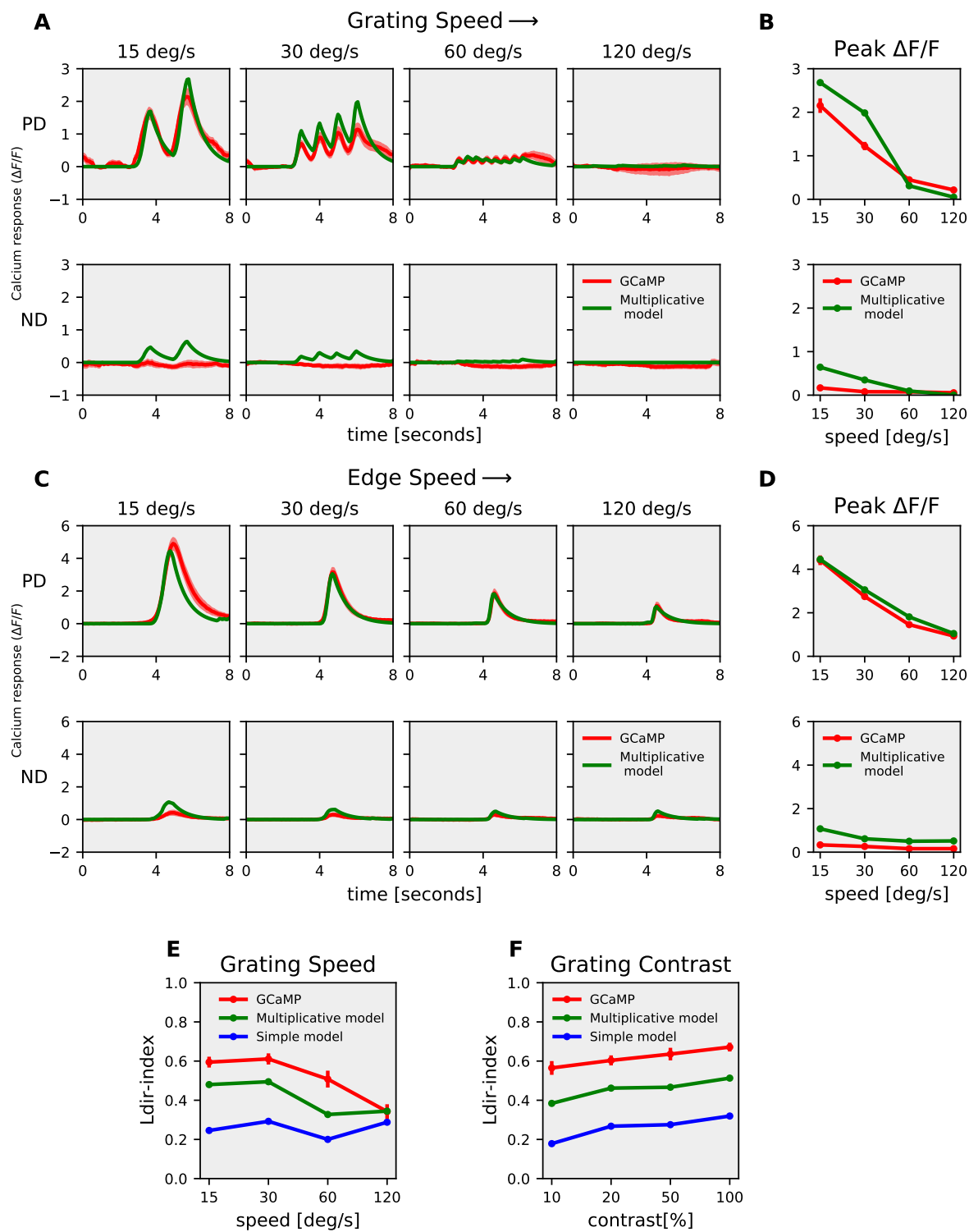


Figure 5. Model responses : (A) T4c GCaMP6f (red) and multiplicative model (green) responses to grating moving in PD (top row) and ND (bottom row) at 4 different speeds. (B) T4c GCaMP6f and model peak responses to grating moving in PD (top) and ND (bottom) at 4 different speeds. (C) T4c GCaMP6f (red) and multiplicative model (green) responses to ON-edge moving in PD (top row) and ND (bottom row) at 4 different speeds. (D) T4c GCaMP6f and model peak responses to ON-edge moving in PD (top) and ND (bottom) at 4 different speeds. (E, F) The directional tuning index L_{dir} for GCaMP6f (red), multiplicative (green) and simple (blue) model for grating moving in 12 directions at 4 different speeds and at 4 different contrasts respectively.

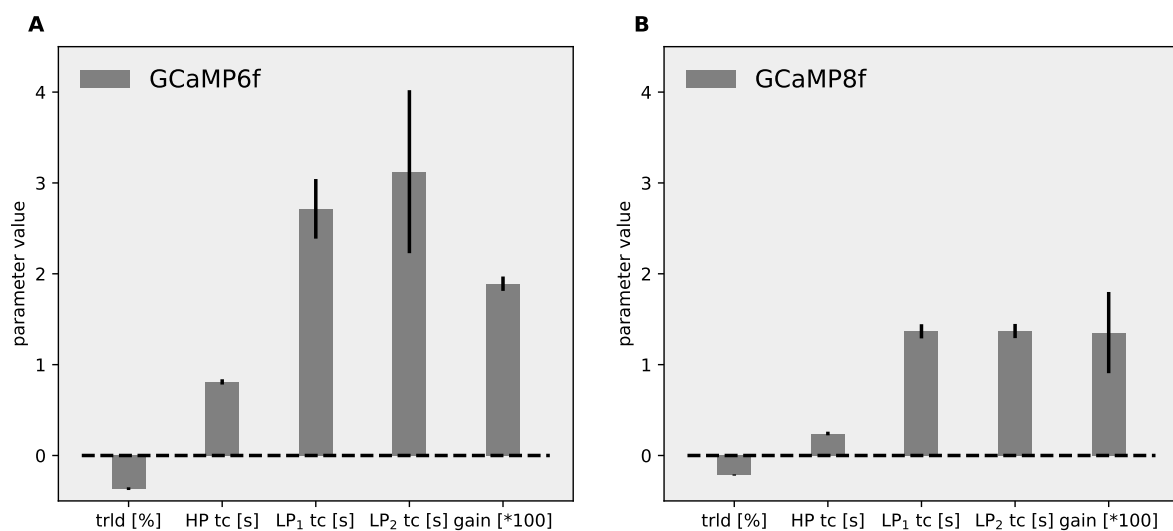


Figure 6. Model parameters for GCaMP6f (A) and GCaMP8f (B) : Data shows mean \pm SD for optimal parameters for the multiplicative model. The data were fit for grating moving in 12 directions and 4 speeds, and for ON-edge moving in PD and ND at 4 speeds. trld : threshold, HP : High Pass, LP : Low Pass, tc : Time constant

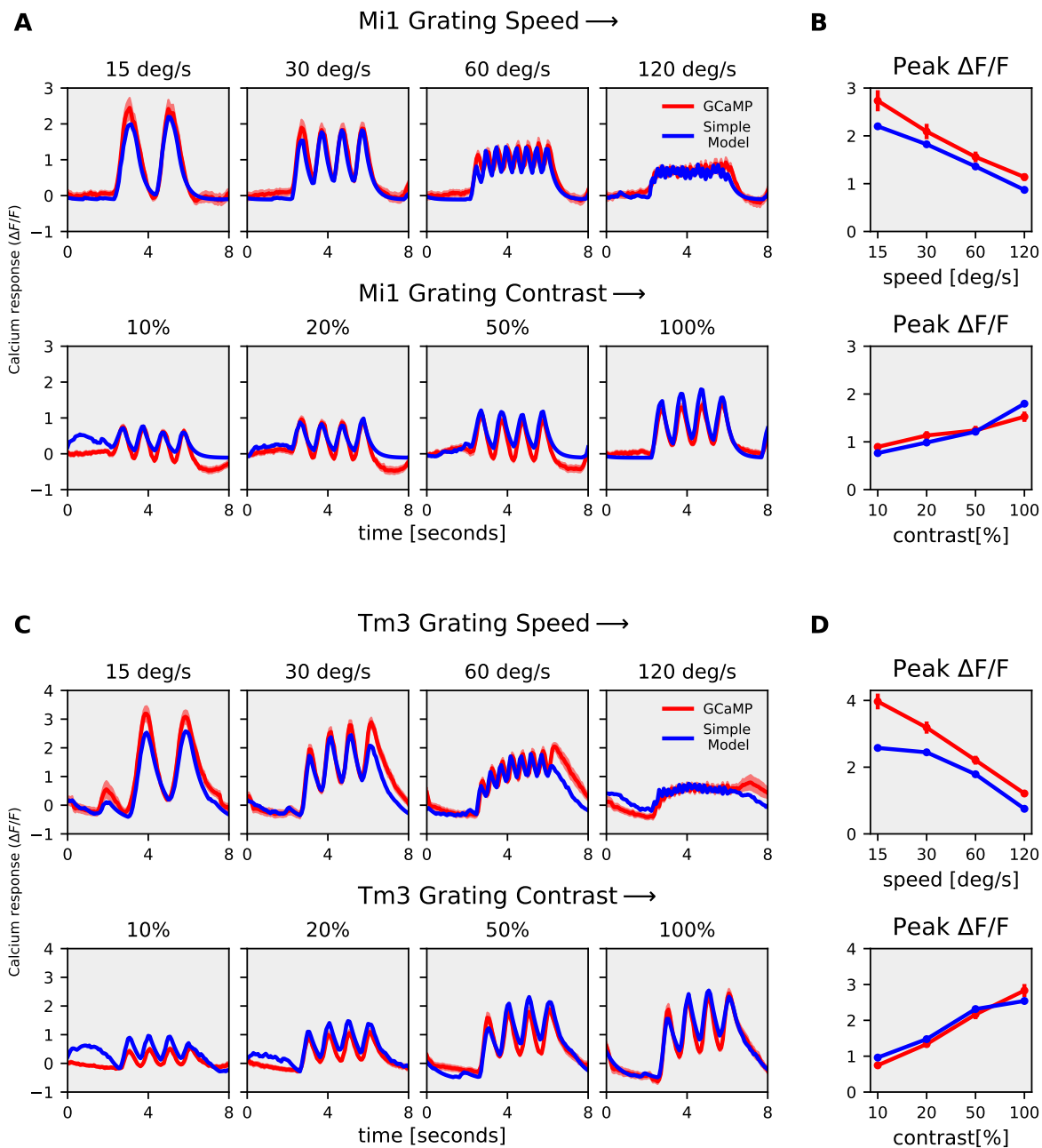


Figure 8. Mi1, Tm3 Simple model responses : (A) Mi1 GCaMP6f (red) and simple model (blue) responses to gratings moving at 4 different speeds (top row) and to gratings moving at 4 different contrasts (bottom row). (B) Mi1 GCaMP6f and model peak responses to gratings moving at 4 different speeds (top) and 4 different contrasts (bottom). (C) Tm3 GCaMP6f (red) and simple model (blue) responses to gratings moving at 4 different speeds (top row) and to gratings moving at 4 different contrasts (bottom row). (D) Tm3 GCaMP6f and model peak responses to gratings moving at 4 different speeds (top) and 4 different contrasts (bottom).

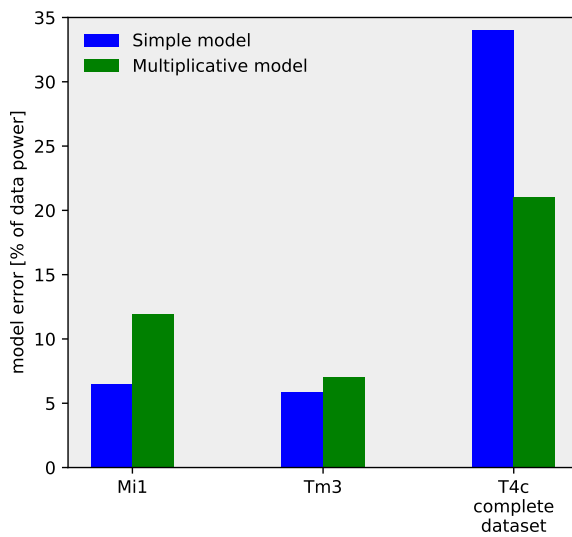


Figure 9. Model error for the simple and multiplicative model : The model error for the simple model (blue) and multiplicative model (green). Mi1 and Tm3 dataset consists of gratings at 4 different speeds and contrast moving in a single direction. T4c complete dataset consists of gratings moving in 12 different directions, and ON edge moving in PD, ND at 4 different speeds and contrasts i.e. a total of 112 stimuli conditions.